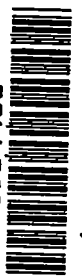


NACA TN 3188 0876

TECH LIBRARY KAFB, NM  
0066081



# NATIONAL ADVISORY COMMITTEE FOR AERONAUTICS

TECHNICAL NOTE 3188

AN ANALYTICAL INVESTIGATION OF AIRPLANE SPIN-RECOVERY  
MOTION BY USE OF ROTARY-BALANCE AERODYNAMIC DATA

By Stanley H. Scher

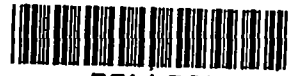
Langley Aeronautical Laboratory  
Langley Field, Va.



Washington

June 1954

AFMDC  
TECHNICAL  
AFL 201



## TECHNICAL NOTE 3188

## AN ANALYTICAL INVESTIGATION OF AIRPLANE SPIN-RECOVERY

## MOTION BY USE OF ROTARY-BALANCE AERODYNAMIC DATA

By Stanley H. Scher

## SUMMARY

A preliminary calculation of an airplane spin-recovery motion has been made and the calculation technique has been evaluated as a possible means for investigating spin and recovery motions for extreme flight conditions difficult or impossible to simulate by free-spinning-tunnel tests. The recovery was calculated step by step by using modified wind-tunnel rotary-balance measurements, applicable equations of motion, and spin-geometry relationships. Difficulties encountered in using the rotary-balance data in the calculations are discussed, and it is pointed out that certain inconsistencies must be cleared up before the method can be accepted as adequate to give detailed spin-recovery motions for a specific airplane. Time-history plots are presented which represent variations, after rudder reversal for attempted recovery, of ensuing attitudes, velocities, and accelerations of the airplane with respect to the airplane body axes, the earth, the relative wind, and the resultant axis of the spinning motion. The time-history curves indicate initial small oscillations of the factors from their original values, with these oscillations increasing gradually in amplitude and with nearly all the large significant changes occurring near the end of the time required for recovery.

## INTRODUCTION

Many investigations have been made in the Langley 20-foot free-spinning tunnel in which the natures of airplane spins and recoveries have been determined experimentally with dynamically scaled-down models. The results of some of these investigations are presented in references 1 to 5. The trends in airplane design, however, have increased the difficulty of making dynamic-model spin tests and interpreting the results, either because of the nature of the motion obtained or because of tunnel limitations. Determination of spin and recovery motions for some current extreme airplane flight conditions cannot be made by the dynamic-model technique as, for example, motions of airplanes at extremely high altitudes at which the model wing loadings required to simulate the airplanes dynamically are impracticably high for testing in the free-spinning

tunnel. Also, the free-spinning-tunnel technique cannot be used to investigate spinning motions which may be encountered in flight at high Mach numbers. Thus, it appears desirable to be able to determine the motion of an airplane during the spin and recovery analytically.

The results of some previous analytical considerations of spin recovery were reported in reference 6 in which step-by-step calculations were made to study the relative efficiencies of the three airplane controls (rudder, ailerons, and elevator) in achieving recovery from an established spin; however, because of a lack of more complete aerodynamic data, this work was handicapped by the necessity of using estimated aerodynamic forces and moments based on the assumption of constant derivatives. The present investigation is a preliminary evaluation of a calculation technique which makes use of aerodynamic data obtained on a wind-tunnel rotary balance and in which the assumption of constant aerodynamic derivatives is not necessary. In this investigation, applicable equations of motion and spin-geometry relationships were used with the rotary-balance aerodynamic data to calculate step by step the details of a spin-recovery motion for an unswept-wing fighter-airplane configuration. Because of certain inconsistencies in the rotary-balance data (similar to those previously discussed in ref. 7), some modifications were made to the aerodynamic force and moment coefficients used in the calculations. The inconsistencies are believed to be primarily due to difficulties involved in mounting the airplane model in order to obtain correctly the aerodynamic data to simulate a steady spin. These inconsistencies and the modifications are discussed in detail subsequently.

The calculated recovery motion is presented as time-history plots of the variations, after rudder reversal for attempted recovery, of ensuing attitudes, velocities, and accelerations of the airplane with respect to the airplane body axes, the earth, the relative wind, and the resultant axis of the spinning motion.

#### SYMBOLS

The calculated recovery motion is presented with respect to the airplane body system of axes and to space and wind attitude angles (fig. 1) and also with respect to the axis of resultant rotation of the motion.

$C_x$  longitudinal-force coefficient,  $\frac{X}{\frac{1}{2}\rho V_R^2 S}$

$C_y$  lateral-force coefficient,  $\frac{Y}{\frac{1}{2}\rho V_R^2 S}$

|          |                                                                                                                                                                        |
|----------|------------------------------------------------------------------------------------------------------------------------------------------------------------------------|
| $C_Z$    | normal-force coefficient, $\frac{Z}{\frac{1}{2}\rho V_R^2 S}$                                                                                                          |
| $C_L$    | rolling-moment coefficient, $\frac{L}{\frac{1}{2}\rho V_R^2 S b}$                                                                                                      |
| $C_m$    | pitching-moment coefficient, $\frac{M}{\frac{1}{2}\rho V_R^2 S b}$                                                                                                     |
| $C_n$    | yawing-moment coefficient, $\frac{N}{\frac{1}{2}\rho V_R^2 S b}$                                                                                                       |
| X        | longitudinal force, lb                                                                                                                                                 |
| Y        | lateral force, lb                                                                                                                                                      |
| Z        | normal force, lb                                                                                                                                                       |
| F        | resultant force, lb                                                                                                                                                    |
| L        | rolling moment, ft-lb                                                                                                                                                  |
| M        | pitching moment, ft-lb                                                                                                                                                 |
| N        | yawing moment, ft-lb                                                                                                                                                   |
| S        | wing area, sq ft                                                                                                                                                       |
| b        | wing span, ft                                                                                                                                                          |
| $\rho$   | air density, slugs/cu ft                                                                                                                                               |
| u,v,w    | components of resultant linear velocity $V_R$ along the X, Y, and Z body axes, respectively, positive in directions of positive X-, Y-, and Z-forces, ft/sec           |
| $V_R$    | resultant linear velocity of airplane, ft/sec                                                                                                                          |
| p,q,r    | components of resultant angular velocity $\Omega$ about the X, Y, and Z body axes, respectively, positive in directions of positive L-, M-, and N-moments, radians/sec |
| $\Omega$ | resultant angular velocity (if axis of resultant rotation is vertical, $\Omega = \dot{\psi}_e$ ), radians/sec                                                          |

|                          |                                                                                                                                                                                                                                         |
|--------------------------|-----------------------------------------------------------------------------------------------------------------------------------------------------------------------------------------------------------------------------------------|
| $\mu$                    | airplane relative-density coefficient, $\frac{m}{\rho S b}$                                                                                                                                                                             |
| $m$                      | mass of airplane, $\frac{\text{Weight}}{g}$ , slugs                                                                                                                                                                                     |
| $c$                      | local chord, ft                                                                                                                                                                                                                         |
| $\bar{c}$                | mean aerodynamic chord, ft                                                                                                                                                                                                              |
| $x/\bar{c}$              | ratio of distance of center of gravity rearward of leading edge of mean aerodynamic chord to mean aerodynamic chord                                                                                                                     |
| $z/\bar{c}$              | ratio of distance between center of gravity and X body axis to mean aerodynamic chord (positive when center of gravity is below X body axis)                                                                                            |
| $k_X, k_Y, k_Z$          | radii of gyration about X, Y, and Z body axes, respectively, ft                                                                                                                                                                         |
| $I_X, I_Y, I_Z$          | moments of inertia about X, Y, and Z body axes, respectively, slug-ft <sup>2</sup>                                                                                                                                                      |
| $\frac{I_X - I_Y}{mb^2}$ | inertia yawing-moment parameter                                                                                                                                                                                                         |
| $\frac{I_Y - I_Z}{mb^2}$ | inertia rolling-moment parameter                                                                                                                                                                                                        |
| $\frac{I_Z - I_X}{mb^2}$ | inertia pitching-moment parameter                                                                                                                                                                                                       |
| $g$                      | acceleration due to gravity, taken as 32.17 ft/sec <sup>2</sup>                                                                                                                                                                         |
| $\theta_e$               | vertical component of total angular deflection of X body axis from a reference position in horizontal plane, positive when sense of deflection is airplane nose upward from reference position, deg or radians as indicated (fig. 1(a)) |
| $\psi_e$                 | horizontal component of total angular deflection of X body axis from reference position in horizontal plane, positive when clockwise as viewed from vertically above airplane, deg or radians as indicated (fig. 1(b))                  |

- $\phi_e$  component in YZ body plane of angular deflection of Y body axis from horizontal plane, positive when clockwise as viewed from rear of airplane (if X body axis is vertical,  $\phi_e$  is measured in horizontal plane), deg or radians as indicated (fig. 1(c))
- $\phi$  angle between Y body axis and horizontal, positive for erect spins when right wing is down and for inverted spins when left wing is down, deg
- $\phi'$  acute angle between Y body axis and a plane perpendicular to axis of resultant rotation,  $\sin^{-1} \frac{q}{\Omega}$ , deg
- $\alpha_1$  acute angle between X body axis and vertical, deg
- $\alpha_3$  acute angle between Z body axis and horizontal, deg
- $\alpha_1'$  angle between X body axis and axis of resultant rotation,  $\cos^{-1} \frac{p}{\Omega}$  or  $\sin^{-1} \frac{\sqrt{r^2 + q^2}}{\Omega}$ , deg
- $\alpha$  angle of attack between relative wind  $V_R$  projected into XZ plane of symmetry and X body axis, positive when relative wind comes from below XY body plane, deg
- $\beta$  angle of sideslip at center of gravity (angle between relative wind  $V_R$  and XZ plane of symmetry), positive when relative wind comes from right side of plane of symmetry, deg
- $\tau_{V_R}$  angle of inclination of relative wind  $V_R$  from XY body plane, positive when inclined below XY body plane,  $\sin^{-1} \frac{w}{V_R}$ , deg
- $\delta_{V_R}$  angle between relative wind  $V_R$  projected into XY body plane and X body axis, positive when  $V_R$  comes from right side of plane of symmetry,  $\sin^{-1} \frac{v}{V_R}$ , deg
- $\tau_{\Omega}$  angle of inclination of axis of resultant rotation from XY body plane, positive when inclined below XY body plane,  $\sin^{-1} \frac{r}{\Omega}$ , deg

|                   |                                                                                                                                                                                                                                 |
|-------------------|---------------------------------------------------------------------------------------------------------------------------------------------------------------------------------------------------------------------------------|
| $\delta_{\Omega}$ | angle between axis of resultant rotation projected into XY body plane and X body axis, positive when vector of axis of resultant rotation lies on right side of plane of symmetry, $\sin^{-1} \frac{q}{\sqrt{p^2 + q^2}}$ , deg |
| $\angle F_2$      | angle of inclination of resultant force vector from XY body plane, positive when inclined below XY body plane, deg                                                                                                              |
| $\angle F_1$      | angle between resultant force vector projected into XY body plane and X body axis, positive when resultant force vector comes from right side of plane of symmetry, deg                                                         |
| t                 | time, sec                                                                                                                                                                                                                       |
| $\Delta t$        | time increment, sec                                                                                                                                                                                                             |
| R                 | spin radius in developed spin, distance from spin axis to center of gravity, ft                                                                                                                                                 |
| $\sigma$          | angle between direction of resultant linear velocity and axis of resultant rotation (helix angle in developed spin), deg                                                                                                        |
| V                 | velocity of airplane center of gravity along axis of resultant rotation, $V_R \cos \sigma$ , ft/sec                                                                                                                             |
| $\kappa_{\Omega}$ | angle between axis of resultant rotation and vertical, deg                                                                                                                                                                      |
| $\kappa_{V_R}$    | angle between resultant linear velocity and vertical, deg                                                                                                                                                                       |
| I,II,III,IV,V     | auxiliary angles in spherical triangles used in determining $\sigma$ (fig. 6) and $\kappa_{\Omega}$ (appendix B), deg                                                                                                           |
| $V_V$             | vertical component of velocity of airplane center of gravity, ft/sec                                                                                                                                                            |
| Subscripts:       |                                                                                                                                                                                                                                 |
| n                 | indicates end of time increment                                                                                                                                                                                                 |
| n-1               | indicates beginning of time increment                                                                                                                                                                                           |

A dot over a symbol represents derivatives with respect to time; for example,  $\dot{u} = \frac{du}{dt}$ .

The attitude angles  $\theta_e$ ,  $\psi_e$ , and  $\phi_e$  (Euler's space angles) as defined and used herein are intended to provide a means of interpreting any changes from the reference attitudes for either an initially erect or an initially inverted spin. Under this general system, the reference attitude for  $\phi_e$  is arbitrarily taken as zero for either an erect or an inverted spin; the airplane would go from an erect to an inverted attitude or vice versa if  $\theta_e$  becomes greater negatively than  $-90^\circ$  or if  $\phi_e$  exceeds  $\pm 90^\circ$ .

#### GENERAL CONSIDERATIONS

A spin is, in general, a motion in which an airplane in flight descends rapidly toward the earth while rotating with angular velocity  $\dot{\psi}_e$  about a vertical axis and while at an angle of attack above that at which the stall occurs. The spin, depending upon the attitude of the airplane in space, may be erect or inverted. If the spin is erect, the angle of attack is positive and, if the spin is inverted, the angle of attack is negative. The airplane must be designed so that recovery from a spin (either erect or inverted) can be achieved following prescribed manipulations of the airplane controls to enable the pilot to regain normal control of the airplane. The motion of a specific airplane during a recovery is apparently dependent on the spin motion before the controls are moved, on the particular control manipulation employed for recovery, and on the effectiveness of these controls (refs. 2 to 5).

Based on dynamic tests on many models in the Langley free-spinning tunnel, it appears that the motion following control movement for recovery may be extremely varied. The variations may range from a motion in which the model, immediately after control movement, decreases its rate of rotation and noses down rapidly for a recovery to one in which movement of the controls has little or no effect on the spinning motion. In some instances, after controls are moved for recovery, oscillations may occur in the attitude of the model and in its rate of rotation, with an over-all trend toward a decrease in both rate of rotation and angle of attack which eventually evolves into a steep low-angle-of-attack pull-out dive without rotation ( $\dot{\psi}_e$  becomes zero). Recovery, however, is sometimes considered as having been achieved if the model appears to have entered a spiral glide or an aileron roll at an angle of attack below the stall. In some cases, recovery from the spin may be associated with a quick rolling or pitching motion to an inverted attitude, and recovery is considered to have been achieved from the original erect spin regardless of whether  $\dot{\psi}_e$  has changed its direction in space. From a practical standpoint it would be necessary that the pilot of a corresponding airplane be able to exercise sufficient care to avoid entering another spin after having achieved recovery from an original spin. These general considerations would also apply were the original spin inverted rather than erect.

When a free-spinning-tunnel model has recovered from a spin within  $2\frac{1}{4}$  turns after control manipulation, the airplane being simulated by the model is customarily considered to have satisfactory spin-recovery characteristics. This figure has been deduced from experience and is based on comparisons between free-spinning-tunnel test results and available full-scale-airplane spin data.

#### METHODS AND CALCULATIONS

The airplane is considered as a rigid body in space having six degrees of freedom. Equations of motion are used which relate the linear and angular velocities of the airplane along and about the airplane body axes to the attitude of the airplane with respect to the earth. The equations are equivalent to equations given in reference 8 and in various dynamics texts, except that no product of inertia terms appear because the airplane body axes are assumed to be the principal axes. The equations are

$$\dot{u} = \frac{V_R^2}{2\mu b} C_X - g \sin \theta_e + vr - wq$$

$$\dot{v} = \frac{V_R^2}{2\mu b} C_Y + g \cos \theta_e \sin \phi_e + wp - ur$$

$$\dot{w} = \frac{V_R^2}{2\mu b} C_Z + g \cos \theta_e \cos \phi_e + uq - vp$$

$$\dot{p} = \frac{V_R^2}{2\mu k_X^2} C_l + \frac{I_Y - I_Z}{I_X} qr$$

$$\dot{q} = \frac{V_R^2}{2\mu k_Y^2} C_m + \frac{I_Z - I_X}{I_Y} rp$$

$$\dot{r} = \frac{V_R^2}{2\mu k_Z^2} C_n + \frac{I_X - I_Y}{I_Z} pq$$

The airplane is considered to be initially in an erect steady spin turning to the pilot's right in space (positive  $\psi_e$ ). Since in a steady motion

all time derivatives of the variables are zero, the equations of motion show that  $\theta_e$  and  $\phi_e$  must be constant during a steady spin. Therefore, inasmuch as  $\dot{\theta}_e$  and  $\dot{\phi}_e$  are zero, all the spin rotation in terms of Euler's angles must be due to  $\dot{\psi}_e$ , which is a rotation about a vertical axis. The components of the total angular velocity about airplane body axes are given in terms of the rates of change of the Euler angles by the relationships (ref. 9)

$$p = \dot{\phi}_e - \dot{\psi}_e \sin \theta_e$$

$$q = \dot{\theta}_e \cos \phi_e + \dot{\psi}_e \cos \theta_e \sin \phi_e$$

$$r = -\dot{\theta}_e \sin \phi_e + \dot{\psi}_e \cos \theta_e \cos \phi_e$$

These relationships for  $p$ ,  $q$ , and  $r$  and the following relationships were used to find values for  $\phi_e$  and for the velocity factors in the equations of motion when time equaled zero:

$$\phi_e = \sin^{-1} \frac{\sin \phi}{\cos \theta_e} \quad (\text{see fig. 3})$$

$$V_R = \sqrt{V_V^2 + (R\dot{\psi}_e)^2}$$

$$v = V_R \sin \beta$$

$$u = V_R \cos \beta \cos \alpha$$

and

$$w = u \tan \alpha = V_R \cos \beta \sin \alpha$$

where

$$R \approx \frac{g \tan \theta_e}{\dot{\psi}_e}$$

$$\beta \approx \phi - \sigma$$

$$\alpha \approx 90 - \theta_e$$

$$\sigma \approx \tan^{-1} \frac{R\dot{\psi}_e}{V_V}$$

and where  $\theta_e$ ,  $\phi$ ,  $V_V$ , and  $\dot{\psi}_e$  were obtained from available free-spinning-tunnel test results (average values) of a 1/20-scale dynamic model of the airplane being considered.

Mass characteristics and control settings for the airplane and some of the initial erect-spin characteristics are presented in table I. The airplane control manipulation simulated for recovery in the calculations is reversal of the rudder from full with (pro-spin) to full against the spin, with no further control adjustments being simulated.

Unpublished aerodynamic data were available for a 1/10-scale model of the configuration being considered from rotary-balance measurements made in the Langley 20-foot free-spinning tunnel. A drawing of this model is shown in figure 2. The rotary balance used consists of a six-component strain gage that measures forces along the three airplane-model body axes and moments about these three axes while the model is being forcibly rotated at a constant rate about a vertical axis in the vertical airstream of the tunnel. The angles of attack and sideslip of the rotary-balance model may be set at angles from  $0^\circ$  to  $360^\circ$ . A complete description of this rotary balance is contained in reference 7. As obtained, the available rotary-balance data included values of the force and moment coefficients for wide ranges of  $\beta$ ,  $\alpha$ , and  $\Omega$  with the model rudder neutral and also values of the force and moment coefficients for rudder-with and rudder-against conditions at  $0^\circ$  sideslip for the ranges of  $\alpha$  and  $\Omega$ . The control settings used on the model were somewhat different from those used in the free-spinning dynamic-model tests mentioned previously (table I). The model elevator was set at  $30^\circ$  up and the ailerons were set at  $\pm 20^\circ$  against the spin (in corresponding airplane, stick left in spin to pilot's right). All these data were obtained from rotation tests in which the model was rotated about a vertical axis through its center of gravity (zero spin radius).

The aerodynamic data obtained include no effects of accelerations such as are accounted for by the dot stability derivatives in studies of airplane stability or motion. The effect of the lack of these accelerations in obtaining the aerodynamic data is probably negligible when attempting to simulate a fairly steady spin, and although the effects on a calculated spin-recovery motion are not known, they may not be appreciable. In obtaining data with the rotary balance, it should be pointed out that proper settings of the instantaneous spin radius (distance between the instantaneous axis of the rotation and the center of gravity of the

model) and the heading or azimuth angle must be included in order to simulate fully (except for acceleration effects) the motion of a free airplane model in a steady spin or at any instant in the recovery. By using the correct values of the instantaneous spin radius, the azimuth angle, the angles between the model body axes and the instantaneous spin axis, and the tunnel airspeed and by rotating the model at the proper angular velocity, all the variables of the motion (that is,  $u$ ,  $v$ ,  $w$ ,  $p$ ,  $q$ , and  $r$ ) may be obtained simultaneously. At the time the aerodynamic data used in this investigation were accumulated, it appeared as though an impracticably large amount of testing time would be required if the spin radius and heading angle of the model were included as variables in obtaining the data for interpolation; however, previous unpublished work shows that, for apparent steady-spin conditions, rotary-balance measurements with zero spin radius did not differ appreciably from measurements where spin radius was used when  $\alpha$ ,  $\beta$ , and  $\Omega$  were adjusted to be the same for the two conditions. If the radius of turn should become relatively very large, however, as it may near the end of a recovery, the use of zero-spin-radius rotary-balance data in calculating the spin recovery may have some effect on that part of the calculated motion.

In a previous investigation (ref. 7) in which the rotary balance was used to measure the aerodynamic forces and moments under conditions which were representative of apparently steady spins in the free-spinning tunnel, even though spin radius was used, the values obtained for the aerodynamic forces and moments were found to be inconsistent with the assumption of a steady spin in that the aerodynamic and inertial forces and moments did not balance. Because of this discrepancy either the aerodynamic data or the inertial characteristics must be modified to simulate equilibrium in the steady spinning condition. For the present investigation also, the inertial and aerodynamic forces and moments did not balance; thus, the aerodynamic data were arbitrarily modified by adding the proper increment to each force and moment coefficient to obtain equilibrium in the steady spin. During the calculated recovery motion, the aerodynamic data were modified by adding these same increments at each instant. The use of these corrections does not mean that the balance gives erroneous readings, and as mentioned previously, the inconsistencies are believed to be due to difficulties involved in mounting the model.

The increments added to the force and moment coefficients to obtain equilibrium in the free-spinning condition at  $t = 0$  were evaluated as follows: The rudder-neutral aerodynamic coefficients for the free-spinning condition were obtained from the tabulated rudder-neutral rotary-balance measurements by interpolating for the proper values of  $\alpha$ ,  $\beta$ , and  $\Omega$ . Since the free-spinning condition had occurred when the rudder was deflected in the pro-spin direction, the proper rudder-with-spin increment was then added to each aerodynamic coefficient. This increment was obtained from the tabulated rotary-balance measurements of rudder-with-spin increments by interpolating for the proper values of  $\alpha$  and  $\Omega$ . The

rudder-deflection increments were assumed to be constant with  $\beta$ . The necessary equilibrium aerodynamic increments were obtained by subtracting the rudder-with-spin aerodynamic coefficients from the free-spinning model inertial coefficients.

At  $t = 0$  the spin-recovery motion was initiated by throwing the rudder against the spin. In the equations of motion, this initiation of the spin recovery was accomplished by subtracting the rudder-with-spin increments from the equilibrium aerodynamic coefficients and then adding the rudder-against-spin increments. The values for the attitudes, velocities, and rudder-against-spin aerodynamic-coefficient factors when time equaled zero were substituted into the equations of motion along with the mass factors of table I, and initial values of  $\dot{u}$ ,  $\dot{v}$ ,  $\dot{w}$ ,  $\dot{p}$ ,  $\dot{q}$ , and  $\dot{r}$  were calculated. These values were assumed to remain constant over a small increment of time, and new values of the velocity terms at the end of the small time increment were calculated by standard acceleration-velocity relationships such as

$$u_n = u_{n-1} + \dot{u}\Delta t$$

and

$$p_n = p_{n-1} + \dot{p}\Delta t$$

New values of the attitude terms in the equations of motion at the end of the small time increment were calculated by the relationships

$$(-\sin \theta_e)_n = (-\sin \theta_e)_{n-1} + \frac{d(-\sin \theta_e)}{dt} \Delta t$$

$$(\cos \theta_e \sin \phi_e)_n = (\cos \theta_e \sin \phi_e)_{n-1} + \frac{d(\cos \theta_e \sin \phi_e)}{dt} \Delta t$$

and

$$(\cos \theta_e \cos \phi_e)_n = (\cos \theta_e \cos \phi_e)_{n-1} + \frac{d(\cos \theta_e \cos \phi_e)}{dt} \Delta t$$

where the last term in each relationship was assumed to remain constant over the small time increment. Values for these last terms were

determined by the method presented in appendix A. A new value of  $V_R$  was obtained by calculating the vectorial sum of the new values of  $u$ ,  $v$ , and  $w$ . New values of the aerodynamic force and moment coefficients at the end of the small time interval were obtained from the rotary-balance data in a manner similar to that discussed previously for obtaining the coefficients at zero time: namely, the same interpolative procedures were used in the rudder-neutral data, increments were added to the coefficients to account for the rudder being against the spin, and the same correction factors (arbitrarily assumed to be constant correction factors to the balance data) already discussed as being necessary for equilibrium were added. The new values of  $\alpha$  and  $\beta$  needed for making the interpolations were determined by using the new values of linear velocities in the formulas noted previously which relate  $u$ ,  $v$ ,  $w$ , and  $V_R$  to  $\alpha$  and  $\beta$ . The new value of  $\Omega$  needed for making the interpolations was taken as the vectorial sum of the new values of  $p$ ,  $q$ , and  $r$ .

The step-calculation process was repeated many times to obtain time histories of the individual attitude, velocity, and acceleration factors in the equations of motion by substituting the newly obtained values at each step in the right-hand sides of the equations of motion. Time-history plots were made of these variables and also of  $\alpha$ ,  $\beta$ , and  $\Omega$ . A time-history curve indicating the number of spinning turns the model had made in space at any time was obtained from a graphical integration of a curve of  $\dot{\psi}_e$  against time which was calculated by

$$\dot{\psi}_e = \frac{\dot{\phi}_e - p}{\sin \theta_e}$$

a relationship mentioned previously. In the graphical-integration technique, the area under a portion of the curve of  $\dot{\psi}_e$  against time for a given small time increment represented the change occurring in the value of  $\psi_e$  during that time interval.

Time histories for the angles  $\phi$  and  $\phi'$  were calculated from

$$\phi = \sin^{-1} (\sin \phi_e \cos \theta_e) \quad (\text{fig. 3})$$

and

$$\phi' = \sin^{-1} \frac{q}{\Omega}$$

The attitudes of the resultant force vector acting on the airplane, with respect to the XZ and XY body planes, were calculated by (see fig. 4)

$$\angle F_1 = \sin^{-1} \frac{\dot{v} + ur - wp}{\sqrt{(\dot{u} + wq - vr)^2 + (\dot{v} + ur - wp)^2}}$$

and

$$\angle F_2 = \sin^{-1} \frac{\dot{w} + vp - uq}{\sqrt{(\dot{u} + wq - vr)^2 + (\dot{v} + ur - wq)^2 + (\dot{w} + vp - uq)^2}}$$

and the attitudes of the axis of resultant rotation with respect to these planes were calculated by (see fig. 5)

$$\delta_{\Omega} = \sin^{-1} \frac{q}{\sqrt{p^2 + q^2}}$$

and

$$\tau_{\Omega} = \sin^{-1} \frac{r}{\Omega}$$

The angle  $\sigma$  was determined by

$$\cos \sigma = \cos \tau_{\Omega} \cos \tau_{V_R} \cos (\delta_{\Omega} - \delta_{V_R}) + \sin \tau_{\Omega} \sin \tau_{V_R}$$

(fig. 6) and the velocity of the airplane along the axis of resultant rotation was calculated by

$$V = V_R \cos \sigma$$

The inclination of the axis of resultant rotation from the vertical at various times during the recovery was determined by (appendix B)

$$\cos \kappa_{\Omega} = \cos \alpha_1' \cos \alpha_1 + \sin \alpha_1' \sin \alpha_1 \cos III$$

The velocity of descent toward the earth at various times during the recovery was obtained by adding vertical velocity components, as

$$V_V = -u \sin \theta_e + v \cos \theta_e \sin \phi_e + w \cos \theta_e \cos \phi_e$$

and the inclination of the resultant velocity vector from the vertical was calculated by

$$\cos \kappa_{VR} = \frac{V_V}{V_R}$$

The calculations were continued until the plotted time-history curves indicated that the airplane had achieved such an attitude and motion that a recovery from the erect spin had occurred.

### RESULTS AND DISCUSSION

The calculated motion is presented as time-history plots of the various attitude, velocity, and acceleration factors in figures 7 to 15.

Because some of the modifications to the aerodynamic data were relatively large, the detailed calculated recovery motions may not represent those of the model actually tested but may be more representative of the recovery motion of a hypothetical airplane. The adjustments made to the aerodynamic data, however, did not modify the slopes of the aerodynamic data with respect to the variables of the motion and the modifications might be considered as changing the aerodynamic characteristics of the model in order to obtain trim in the observed steady spin; hence, the stability of the airplane in the spin was not affected. The increments in the measured aerodynamic coefficients arising from the rudder deflection and from the changes in the variables of the motion during the recovery do, of course, change the slopes of these aerodynamic coefficients. It is believed that these latter increments and the inertia characteristics of the model were obtained with good accuracy. Therefore, in the event that the stability of the airplane in the spin determines the more important characteristics of the recovery motion, the calculated recovery may fairly well represent that of the actual rotary-balance model tested.

As may be seen from the figures, the plots show initial gentle oscillations from the original values of the attitude, velocity, and acceleration factors, with the oscillations gradually increasing in magnitude with elapsed time. Up to a time of 5 seconds, the changes that occurred in the various factors were relatively small. During the sixth second, large changes occurred. At the end of 6 seconds,  $\phi_e$  had reached a value of  $-97^\circ$  (fig. 7), the angle of attack had reached zero from its original high positive value and was going negative (fig. 8), and  $\dot{\psi}_e$  had almost gone to zero (fig. 9).

These factors and their rates of change indicate that at 6 seconds the airplane had made a rather abrupt left-wing-down rolling motion to a quasi-inverted attitude in space and was still rolling, and recovery from the original spin appeared completed. A pilot in the corresponding airplane should at about this time readjust his controls, probably to neutral or near neutral, to achieve a dive after the recovery motion and to prevent the airplane from entering another developed spin either inverted or erect. The delayed-action, rather abrupt recovery motion indicated by the calculations appears to have its counterpart in the recoveries from spins of some full-scale airplanes. For these airplane recoveries, the controls applied for recovery must be maintained by the pilot for an appreciable amount of time before the spinning motion is affected greatly, after which the recovery occurs rapidly. The rather abrupt left-wing-down rolling motion indicated by the calculations occurred just after  $\phi_e$  (fig. 7) had reached its highest positive value (right wing down) during a phase of the airplane oscillations. From analysis of the rotary-balance data, it appears that this rolling motion was the result of a large negative rolling moment (probably due to the phenomenon of effective dihedral) which built up on the airplane as the inward (positive) sideslip reached a maximum (fig. 8).

An interesting feature of the  $\dot{\psi}_e$  curve (fig. 9) is the sudden large increase which occurred at 5.6 seconds, just before  $\dot{\psi}_e$  decreased rapidly to almost zero. This increase which represents a speeding up of the rotation about a vertical axis was probably associated with the phenomenon of conservation of angular momentum in that it occurred as the airplane pitched down to a steep attitude in space ( $\theta_e$ , fig. 8) and thus decreased the moment of inertia about the vertical axis.

As may be seen from figure 11, the resultant linear velocity  $V_R$  increased slightly above its original value during the recovery. Throughout the recovery motion, the velocity of descent toward the earth  $V_y$  (fig. 15) remained about the same as the resultant velocity  $V_R$ , an indication that the path of the airplane center of gravity and the direction of the resultant wind remained almost vertical. This indication that the resultant wind remained almost vertical is also reflected in the  $\kappa_{V_R}$

curve in figure 15. Figure 12 shows that the resultant force was directed above the XY body plane, forward of the YZ body plane, and alternately to the left and right of the XZ body plane throughout the calculated motion. Figure 13 indicates that during the spin and most of the recovery, the axis of resultant rotation remained almost parallel to the plane of symmetry of the airplane as evidenced by the fact that  $\delta_\Omega$  remained within a few degrees of zero for the first 5 seconds after rudder reversal. Only during the last second of recovery did the axis of resultant rotation deviate appreciably from the plane of symmetry. The angle  $\sigma$  between the resultant linear velocity and the axis of resultant rotation increased a great amount as the motion progressed toward a recovery (fig. 14).

Along with this increase in  $\sigma$ , the velocity component of the airplane parallel to the axis of resultant rotation decreased correspondingly (fig. 15). As  $V$  decreased, the angle  $\kappa_{\Omega}$  between the axis of resultant rotation and the vertical increased until, at the time of the roll-over recovery, the axis of resultant rotation was almost horizontal in space (fig. 15).

The attitude and motion of the airplane at any time during the recovery may be rather completely discerned by simultaneous reference to the time-history curves.

As may be seen from figure 9, the calculations indicated that the airplane made about 2 turns in space while in the recovery motion. Of interest is the fact that the results obtained with the free-spinning-tunnel model mentioned previously also showed an approximately 2-turn recovery. This agreement indicates that the calculation method may give qualitative accuracy in spite of the presently unexplainable equilibrium discrepancies. Any application of this method to obtain the details of a spin recovery for a specific airplane depends on the possibility of explaining these equilibrium discrepancies.

#### CONCLUDING REMARKS

A step-by-step calculation has been made of an airplane spin-recovery motion by use of modified wind-tunnel rotary-balance measurements, applicable equations of motion, and spin-geometry relationships. Difficulties encountered in applying the rotary-balance data in the calculations are discussed, and it is pointed out that certain inconsistencies must be cleared up before the method can be accepted as adequate to give detailed spin-recovery motions for a specific airplane. Time-history plots are presented which represent variations, after rudder reversal for attempted recovery, of ensuing attitudes, velocities, and accelerations of the airplane with respect to the airplane body axes, the earth, the relative wind, and the resultant axis of the spinning motion. The time-history curves indicated initial small oscillations of the factors from their original values, with these oscillations increasing gradually in amplitude and with nearly all the large significant changes occurring near the end of the time required for recovery.

Langley Aeronautical Laboratory,  
National Advisory Committee for Aeronautics,  
Langley Field, Va., March 3, 1954.

## APPENDIX A

## METHOD OF DETERMINING ATTITUDE TERMS

As noted in the body of the paper, expressions for angular velocities about principal axes in terms of Euler's space angles are

$$p = \dot{\phi}_e - \dot{\psi}_e \sin \theta_e$$

$$q = \dot{\theta}_e \cos \phi_e + \dot{\psi}_e \cos \theta_e \sin \phi_e$$

$$r = -\dot{\theta}_e \sin \phi_e + \dot{\psi}_e \cos \theta_e \cos \phi_e$$

Expressing these relationships in terms of  $\dot{\psi}_e$  as

$$\dot{\psi}_e = \frac{\dot{\phi}_e - p}{\sin \theta_e} = \frac{q - \dot{\theta}_e \cos \phi_e}{\cos \theta_e \sin \phi_e} = \frac{r + \dot{\theta}_e \sin \phi_e}{\cos \theta_e \cos \phi_e}$$

and cross-multiplying the resulting equalities, two at a time, gives

$$\cos \theta_e \sin \phi_e (\dot{\phi}_e - p) - \sin \theta_e (q - \dot{\theta}_e \cos \phi_e) = 0$$

$$\cos \theta_e \cos \phi_e (q - \dot{\theta}_e \cos \phi_e) - \cos \theta_e \sin \phi_e (r + \dot{\theta}_e \sin \phi_e) = 0$$

and

$$\cos \theta_e \cos \phi_e (\dot{\phi}_e - p) - \sin \theta_e (r + \dot{\theta}_e \sin \phi_e) = 0$$

When expanded and rearranged these equations become

$$(\cos \theta_e \sin \phi_e \dot{\phi}_e + \sin \theta_e \cos \phi_e \dot{\theta}_e) - p \cos \theta_e \sin \phi_e - q \sin \theta_e = 0$$

$$(-\cos \theta_e \dot{\theta}_e) + q \cos \theta_e \cos \phi_e - r \cos \theta_e \sin \phi_e = 0$$

and

$$(\cos \theta_e \cos \dot{\phi}_e \dot{\theta}_e - \sin \theta_e \sin \dot{\phi}_e \dot{\theta}_e) - p \cos \theta_e \cos \dot{\phi}_e - r \sin \theta_e = 0$$

Replacement of the terms in parentheses by their respective equivalents

$$- \frac{d}{dt}(\cos \theta_e \cos \dot{\phi}_e)$$

$$\frac{d}{dt}(- \sin \theta_e)$$

and

$$\frac{d}{dt}(\cos \theta_e \sin \dot{\phi}_e)$$

gives

$$\frac{d}{dt}(\cos \theta_e \cos \dot{\phi}_e) = - p \cos \theta_e \sin \dot{\phi}_e - q \sin \theta_e$$

$$\frac{d}{dt}(- \sin \theta_e) = - q \cos \theta_e \cos \dot{\phi}_e + r \cos \theta_e \sin \dot{\phi}_e$$

and

$$\frac{d}{dt}(\cos \theta_e \sin \dot{\phi}_e) = p \cos \theta_e \cos \dot{\phi}_e + r \sin \theta_e$$

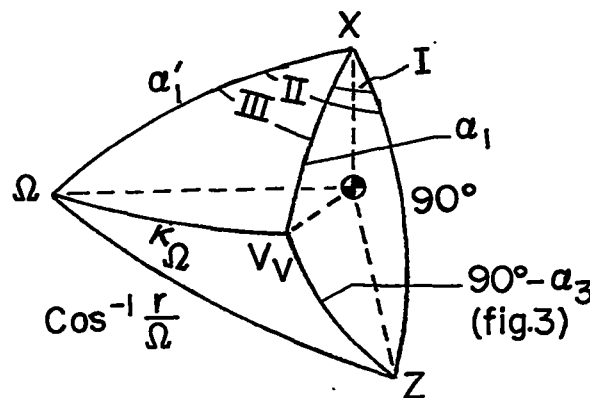
The latter three equations were used to determine values of the left-hand sides at zero time and also at the beginning of each time interval by substituting angular velocity and attitude values at corresponding times in the right-hand sides of the equations.

## APPENDIX B

## METHOD OF DETERMINING INCLINATION OF AXIS OF RESULTANT

## ROTATION FROM VERTICAL

The inclination of the axis of resultant rotation from the vertical was determined by using spherical trigonometry and by making use of the values calculated herein for the inclinations of the axis of resultant rotation with respect to the airplane and for the attitudes of the airplane with respect to the vertical. The method is illustrated by the following sketch and equations which indicate the spherical trigonometrical procedure used for a condition in which the airplane had positive values of  $p$ ,  $q$ , and  $r$  and was in an erect attitude with its right wing somewhat below the horizontal ( $\phi_e$  is positive,  $< 90^\circ$ ). Imagine a sphere of arbitrary radius having its center at the airplane center of gravity. Let points labeled  $X$ ,  $Z$ ,  $\Omega$ , and  $V_V$  in the sketch represent, respectively, points where the surface of the sphere is intersected by the positive directions of the  $X$  and  $Z$  body axes, the axis of resultant rotation, and a vertical line through the center of gravity. The spherical triangles indicated are then created.



As may be seen from the appropriate spherical triangles, the magnitude of angle I may be obtained from

$$\cos(90^\circ - \alpha_3) = \cos 90^\circ \cos \alpha_1 + \sin 90^\circ \sin \alpha_1 \cos I$$

in which

$$\cos I = \frac{\sin \alpha_3}{\sin \alpha_1}$$

the magnitude of angle II may be obtained from

$$\cos \left( \cos^{-1} \frac{r}{\Omega} \right) = \cos \left( \cos^{-1} \frac{p}{\Omega} \right) \cos 90^\circ + \sin 90^\circ \sin \left( \sin^{-1} \frac{\sqrt{r^2 + q^2}}{\Omega} \right) \cos II$$

in which

$$\frac{r}{\Omega} = \frac{\sqrt{r^2 + q^2}}{\Omega} \cos II$$

$$\cos II = \frac{r}{\sqrt{r^2 + q^2}}$$

and the magnitude of angle III from

$$III = II - I$$

Then, as the appropriate spherical triangle in the sketch shows,

$$\cos \kappa_\Omega = \cos \alpha_1^i \cos \alpha_1 + \sin \alpha_1^i \sin \alpha_1 \cos III$$

In using this method care was exercised so that a value of angle III of proper magnitude was obtained for each instant of time at which the angle  $\kappa_\Omega$  was calculated. When the vectors representing a vertical line through the center of gravity and the axis of resultant rotation were on opposite sides of the XZ body plane, a plus sign was required in the formula relating angles III, II, and I to obtain the proper magnitude of angle III. For other possible locations of these vectors not encountered in the present calculated motion, supplementary angles of I and II or both may have to be considered.

## REFERENCES

1. Zimmerman, C. H.: Preliminary Tests in the N.A.C.A. Free-Spinning Wind Tunnel. NACA Rep. 557, 1936.
2. Stone, Ralph W., Jr., and Klinar, Walter J.: The Influence of Very Heavy Fuselage Mass Loadings and Long Nose Lengths Upon Oscillations in the Spin. NACA TN 1510, 1948.
3. Neihouse, Anshal I., Lichtenstein, Jacob H., and Pepon, Philip W.: Tail-Design Requirements for Satisfactory Spin Recovery. NACA TN 1045, 1946.
4. Neihouse, A. I.: Tail-Design Requirements for Satisfactory Spin Recovery for Personal-Owner-Type Light Airplanes. NACA TN 1329, 1947.
5. Neihouse, A. I.: A Mass-Distribution Criterion for Predicting the Effect of Control Manipulation on the Recovery From a Spin. NACA WR L-168, 1942. (Formerly NACA ARR, Aug. 1942.)
6. Bryant, L. W., and Jones, I. M. W.: Notes on Recovery From a Spin. R. & M. No. 1426, British A.R.C., 1932.
7. Stone, Ralph W., Jr., Burk, Sanger M., Jr., and Bihrlle, William, Jr.:  
The Aerodynamic Forces and Moments on a  $\frac{1}{10}$ -Scale Model of a Fighter  
Airplane in Spinning Attitudes as Measured on a Rotary Balance in  
the Langley 20-Foot Free-Spinning Tunnel. NACA TN 2181, 1950.
8. Perkins, Courtland D., and Hage, Robert E.: Airplane Performance - Stability and Control. John Wiley & Sons, Inc., 1949, p. 380.
9. MacMillan, William Duncan: Theoretical Mechanics. Dynamics of Rigid Bodies. First ed., McGraw-Hill Book Co., Inc., 1936, pp. 184-185.

TABLE I.- MASS CHARACTERISTICS, CONTROL SETTINGS, AND  
SPIN CHARACTERISTICS FOR AIRPLANE CONFIGURATION

Mass characteristics:

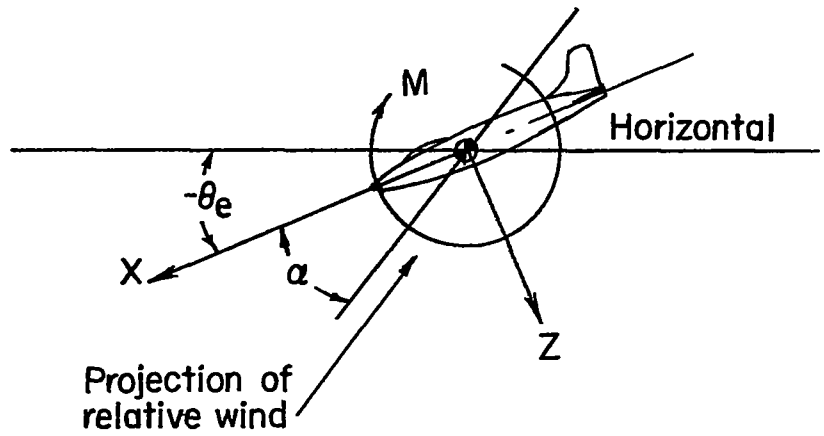
|                                       |                       |
|---------------------------------------|-----------------------|
| Weight, lb . . . . .                  | 17,835                |
| $\frac{x}{c}$ . . . . .               | 0.212                 |
| $\frac{z}{c}$ . . . . .               | 0.009                 |
| $\mu$ at 15,000 ft altitude . . . . . | 17.35                 |
| $I_x$ . . . . .                       | 17,342                |
| $I_y$ . . . . .                       | 37,920                |
| $I_z$ . . . . .                       | 53,396                |
| $\frac{I_x - I_y}{mb^2}$ . . . . .    | $-147 \times 10^{-4}$ |
| $\frac{I_y - I_z}{mb^2}$ . . . . .    | $-110 \times 10^{-4}$ |
| $\frac{I_z - I_x}{mb^2}$ . . . . .    | $257 \times 10^{-4}$  |

Control settings, deg:

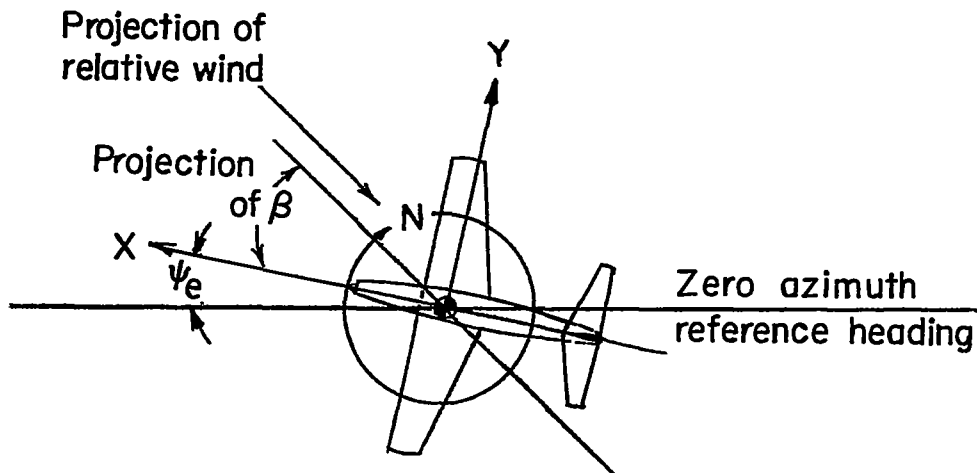
|                                                                           |    |
|---------------------------------------------------------------------------|----|
| Elevator, up (stick back) . . . . .                                       | 20 |
| Ailerons, against spin (stick left in spin to pilot's right) . . .        | 14 |
| Rudder with spin (right pedal forward in spin to pilot's right) . . . . . | 30 |
| Rudder reversed for recovery to against spin . . . . .                    | 30 |

Spin characteristics:

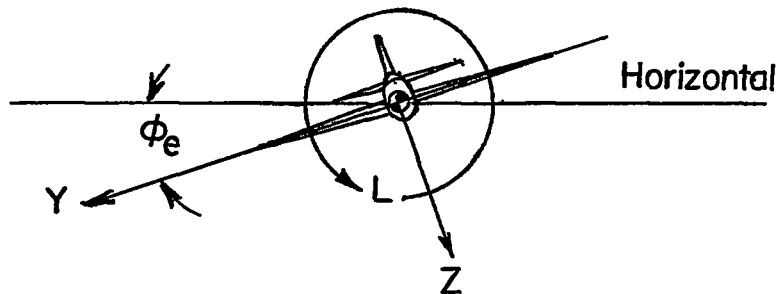
|                                          |       |
|------------------------------------------|-------|
| $\dot{\psi}_e$ , radians/sec . . . . .   | 2.165 |
| $\dot{\theta}_e$ , radians/sec . . . . . | 0     |
| $\dot{\phi}_e$ , radians/sec . . . . .   | 0     |
| $\theta_e$ , deg . . . . .               | -44   |
| $\phi$ , deg . . . . .                   | 0.4   |
| $V_y$ , ft/sec . . . . .                 | 216   |
| R, ft . . . . .                          | 6.62  |
| $\alpha$ , deg . . . . .                 | 46    |
| $\beta$ , deg . . . . .                  | -3.4  |



(a)  $\phi_e$  and  $\psi_e = 0$ .



(b)  $\theta_e$  and  $\phi_e = 0$ .



(c)  $\theta_e$  and  $\psi_e = 0$ , and in this case  $\phi = \phi_e$ .

Figure 1.- Body system of axes and related angles.

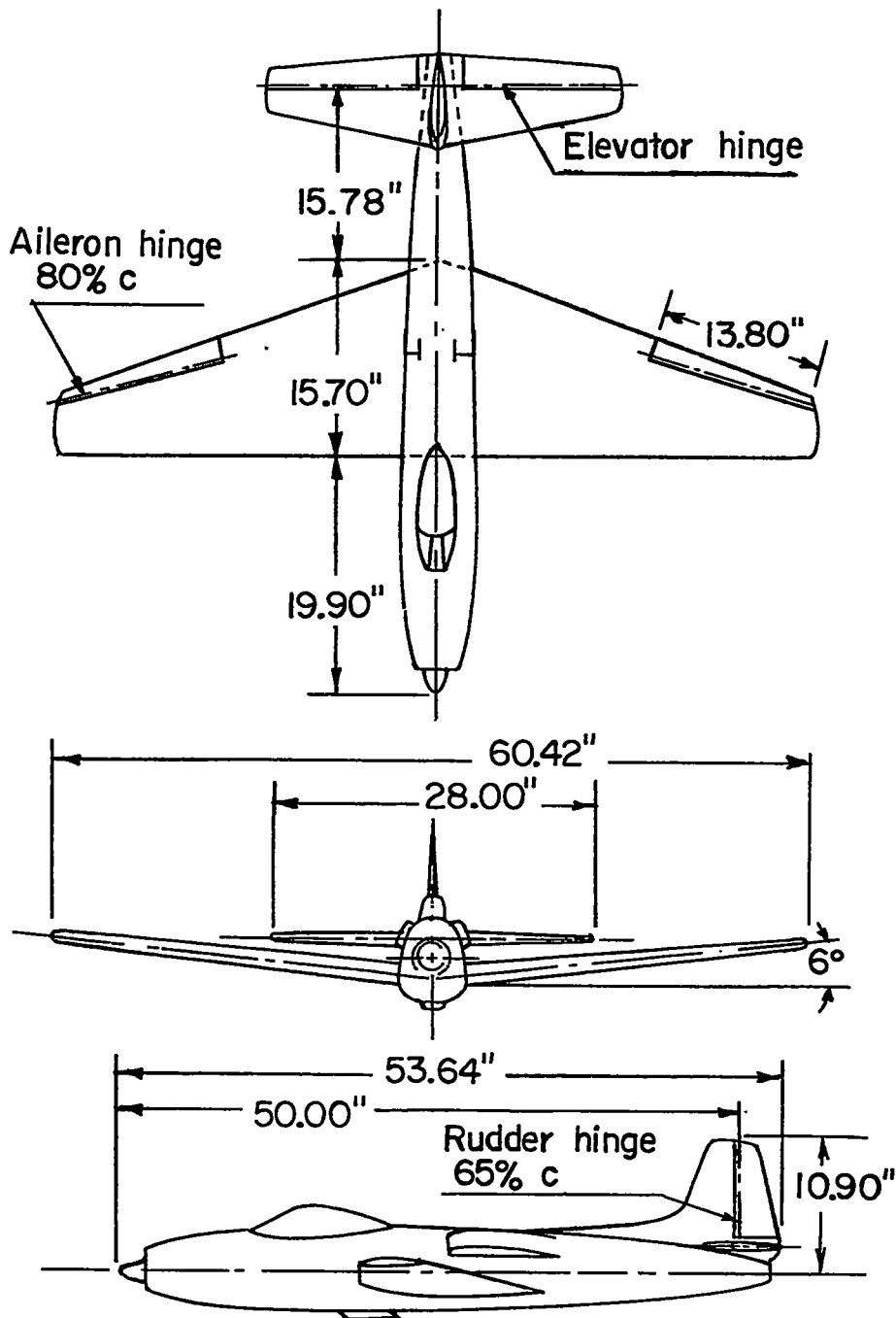


Figure 2.- Rotary-balance model.  $S = 612$  square inches;  $\bar{c} = 11.52$  inches.

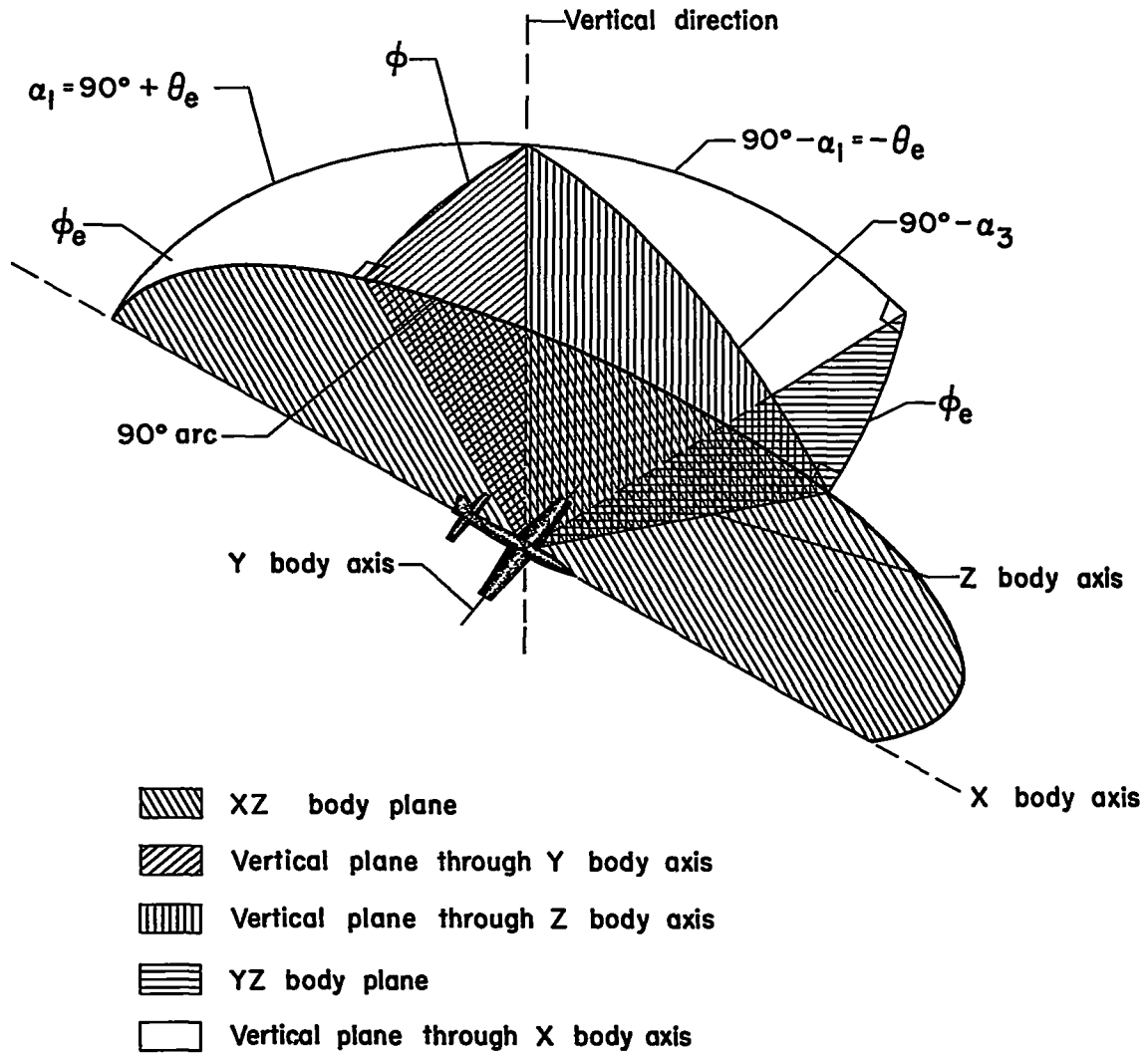


Figure 3.- Sketch indicating spherical trigonometry relationships pertinent to determination of angles  $\phi_e$  and  $\alpha_3$ .  $\sin \phi_e = \frac{\sin \theta}{\cos \theta_e}$ .

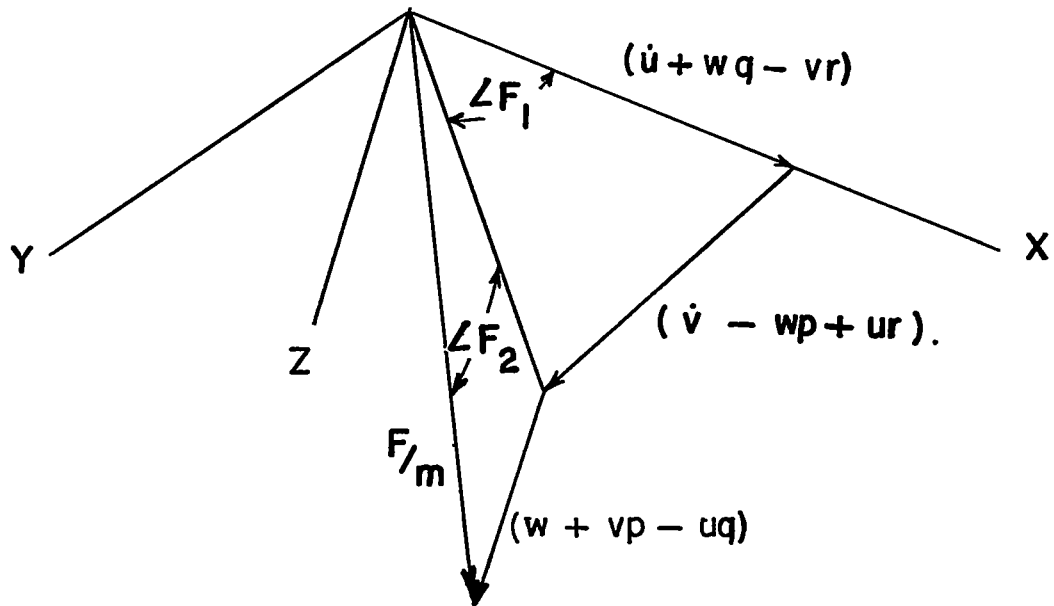


Figure 4.- Vector diagram indicating relationships for obtaining the angles  $\angle F_1$  and  $\angle F_2$ .

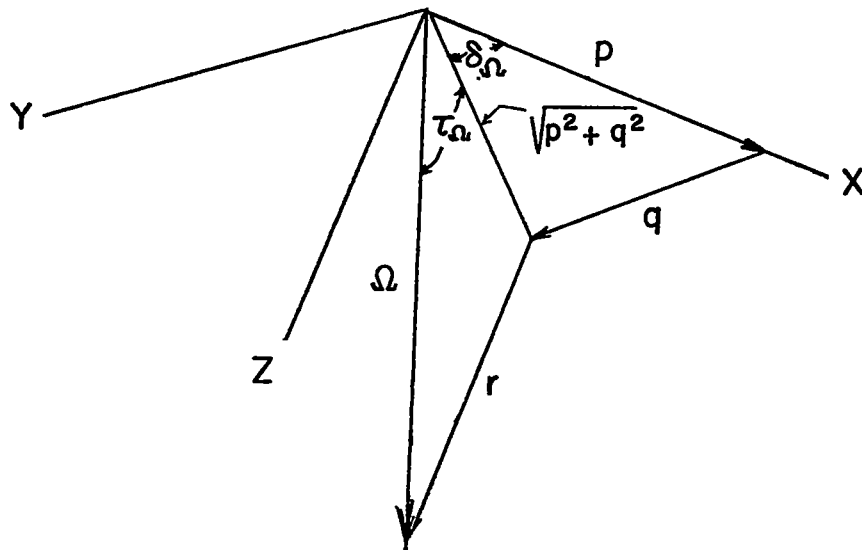
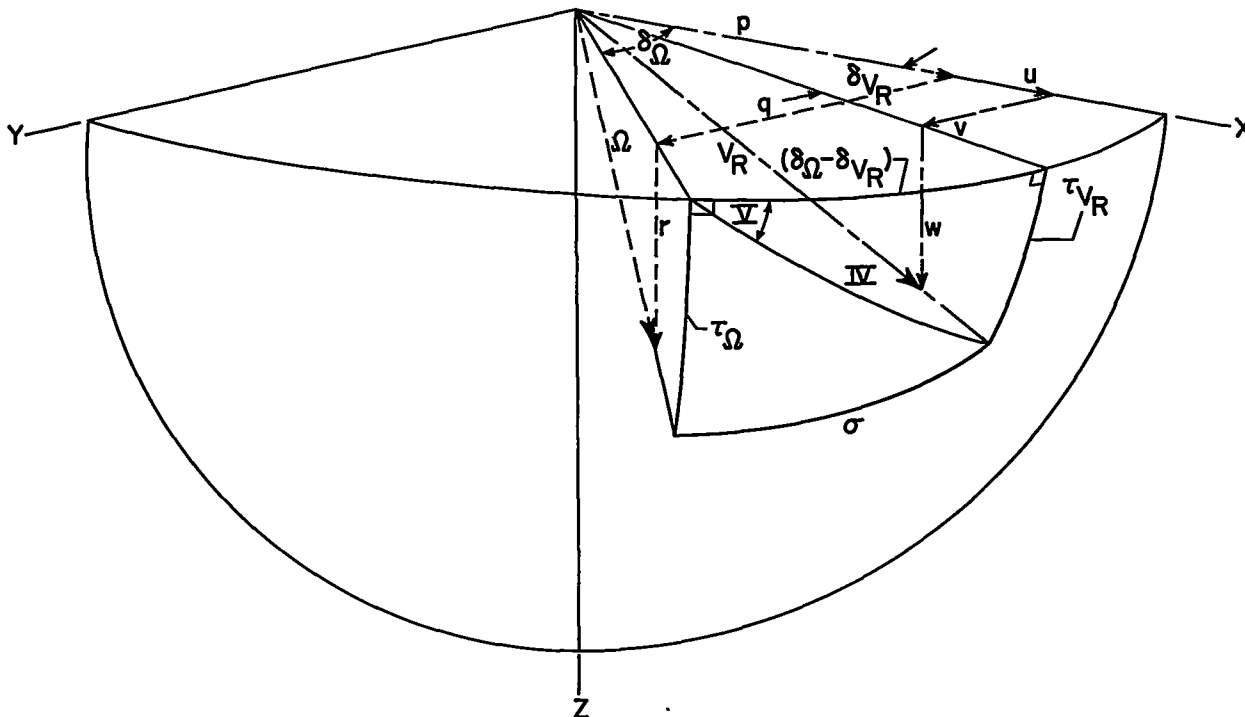


Figure 5.- Vector diagram indicating relationships for obtaining the angles  $\delta_{\Omega}$  and  $\tau_{\Omega}$ .



$$\cos \text{IV} = \cos(\delta_{\Omega} - \delta_{V_R}) \cos \tau_{V_R}$$

$$\sin \text{V} = \frac{\sin \tau_{V_R}}{\sin \text{IV}}$$

$$\cos \sigma = \cos \tau_{\Omega} \cos \text{IV} + \sin \tau_{\Omega} \sin \text{IV} \cos(90^\circ - \text{V})$$

$$\cos \sigma = \cos \tau_{\Omega} \cos \tau_{V_R} \cos(\delta_{\Omega} - \delta_{V_R}) + \sin \tau_{\Omega} \frac{\sin \tau_{V_R}}{\sin \text{V}} \sin \text{V}$$

$$\cos \sigma = \cos \tau_{\Omega} \cos \tau_{V_R} \cos(\delta_{\Omega} - \delta_{V_R}) + \sin \tau_{\Omega} \sin \tau_{V_R}$$

Figure 6.- Sketch indicating vector diagrams and spherical trigonometry relationships pertinent to determination of angle  $\sigma$ .

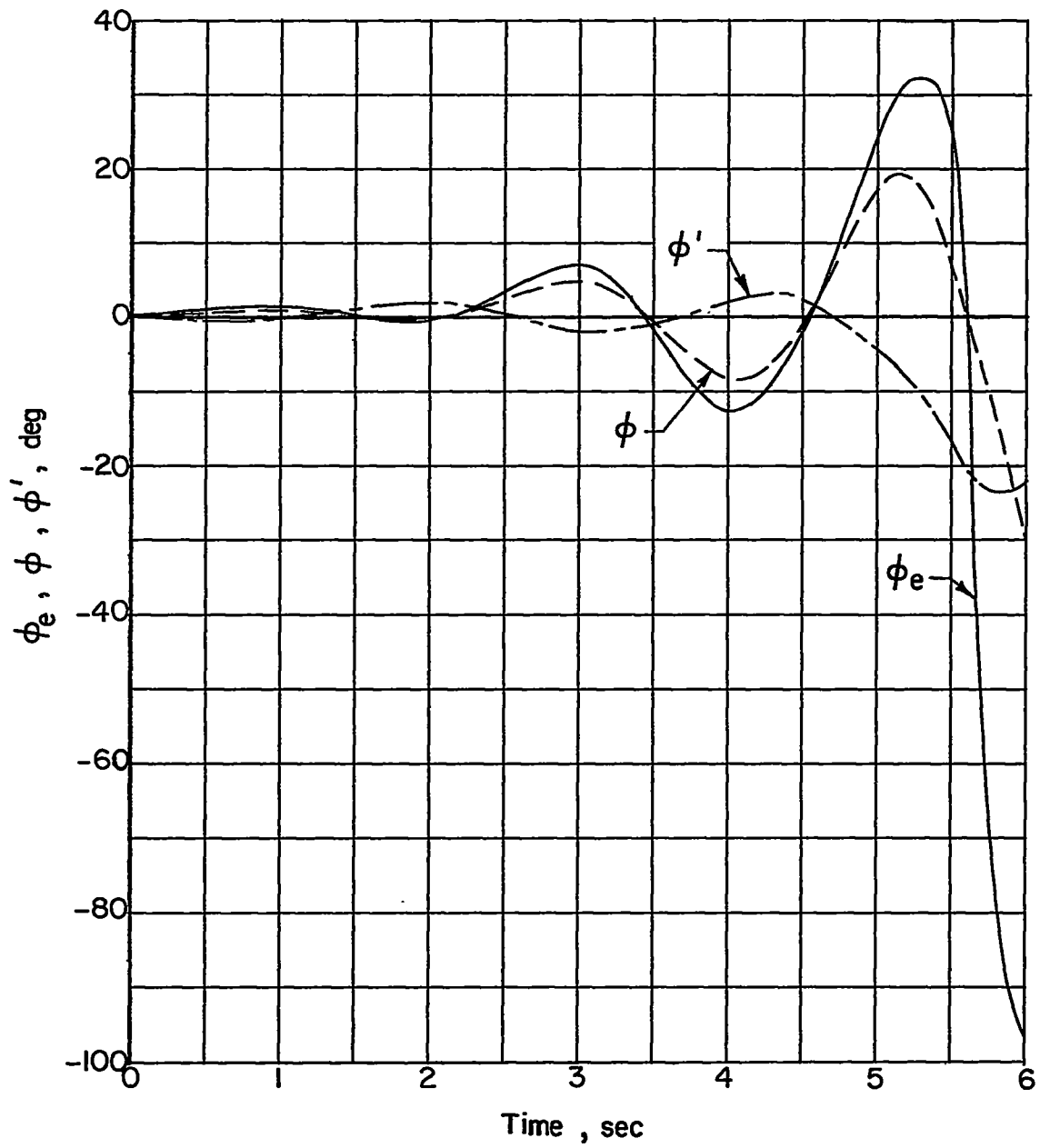


Figure 7.-- Calculated variations of  $\phi_e$ ,  $\phi$ , and  $\phi'$  with time during recovery motion.

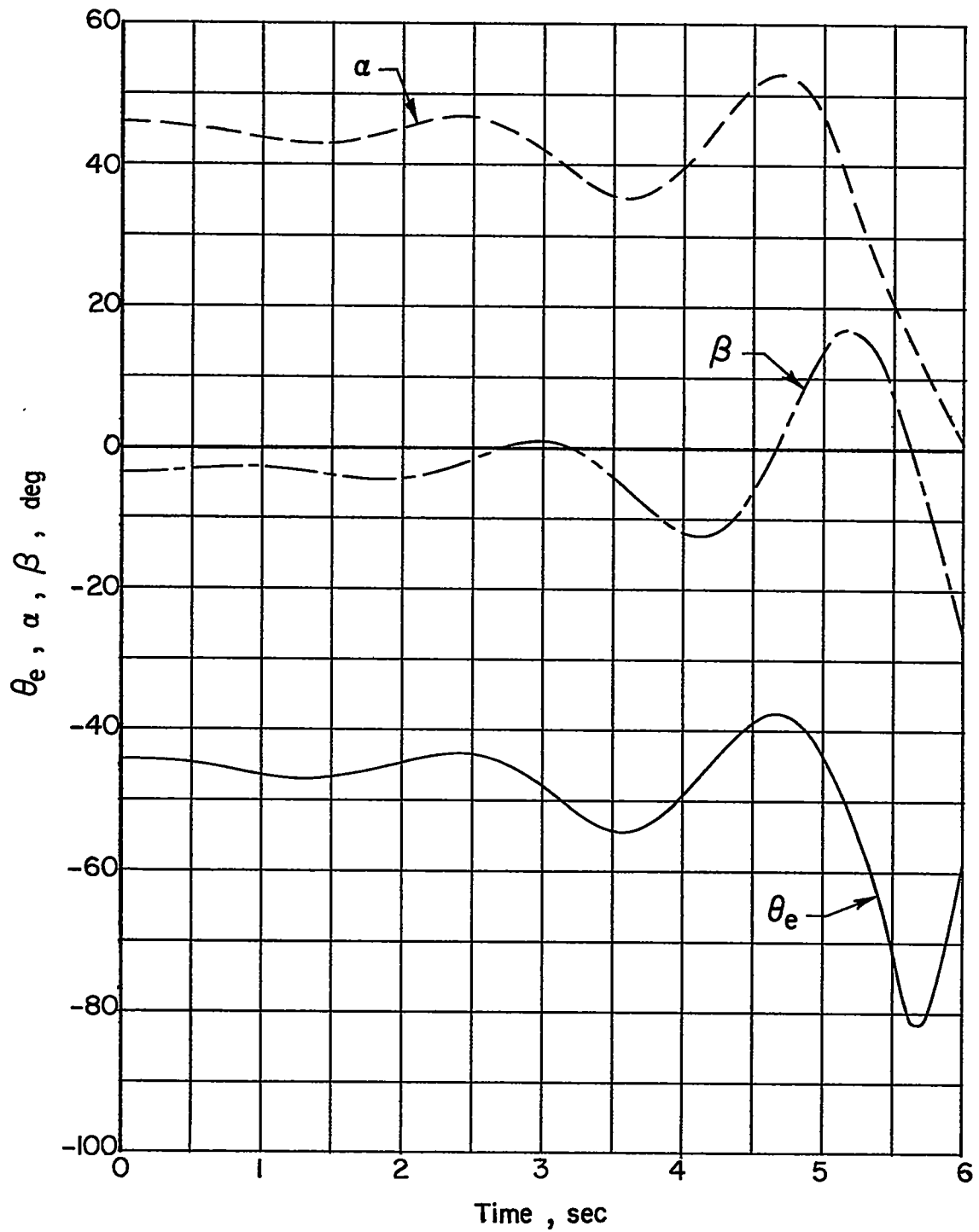


Figure 8.- Calculated variations of  $\theta_e$ ,  $\alpha$ , and  $\beta$  with time during recovery motion.

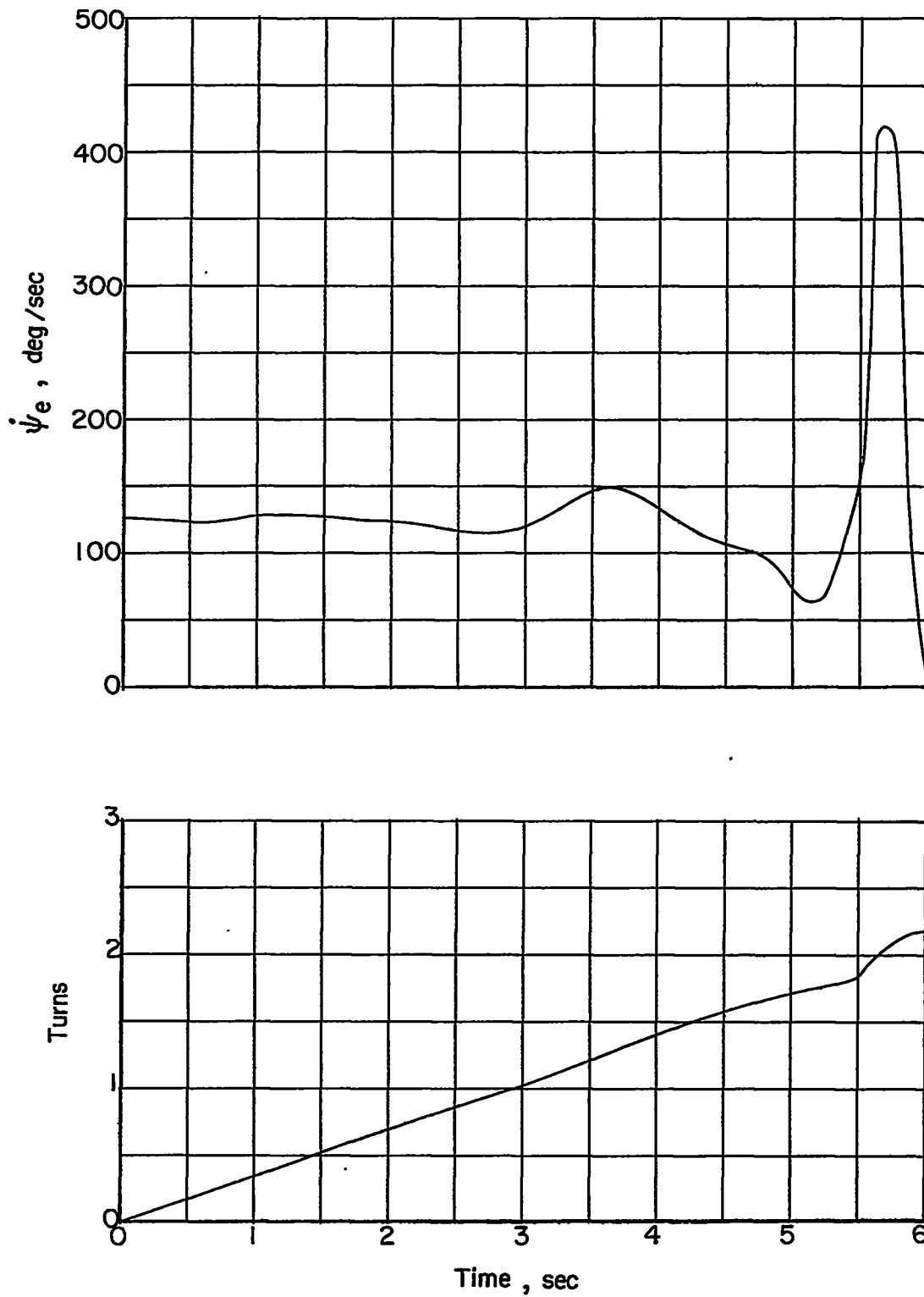


Figure 9.- Calculated variations of  $\dot{\psi}_e$  and turns of model completed in space with time during recovery motion.

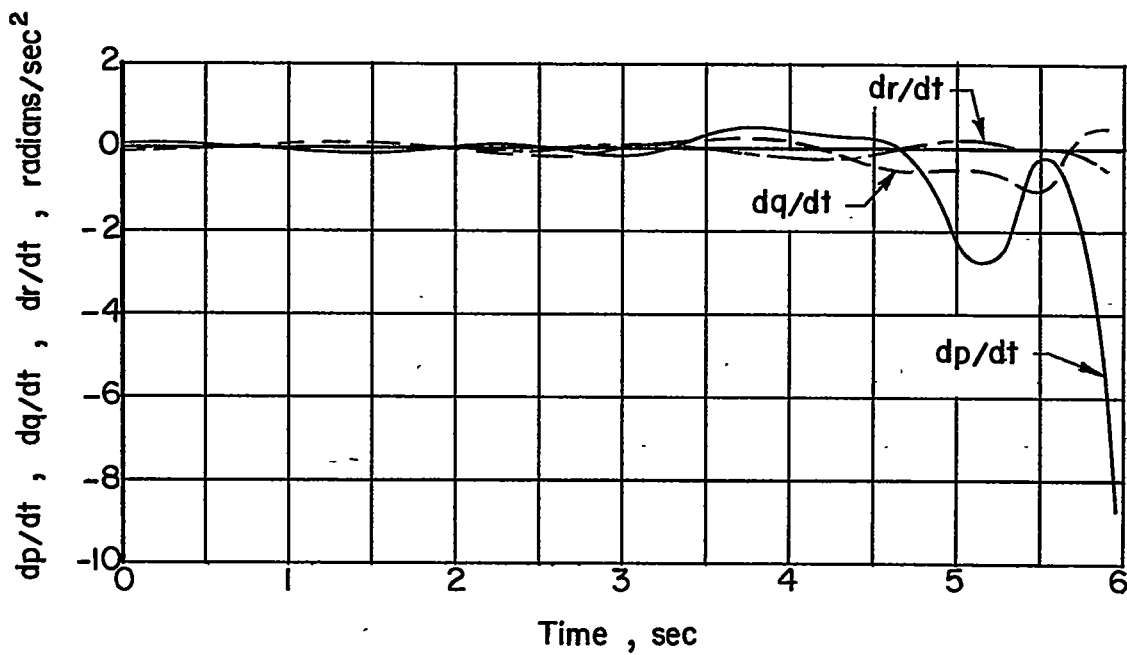
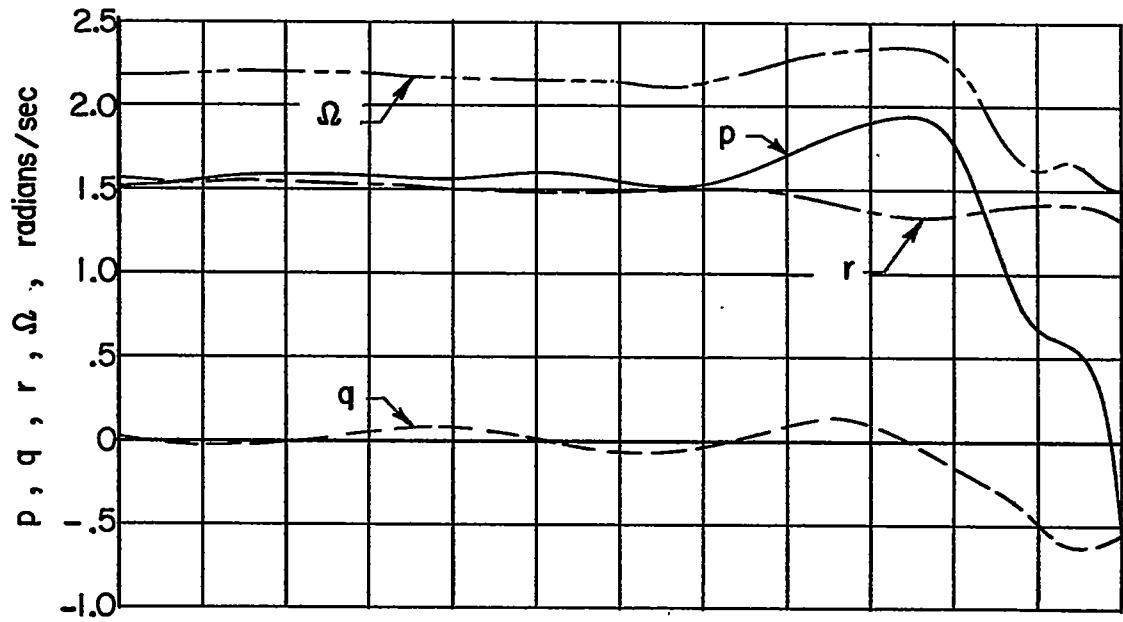


Figure 10.- Calculated variations of angular velocities and accelerations with time during recovery motion.

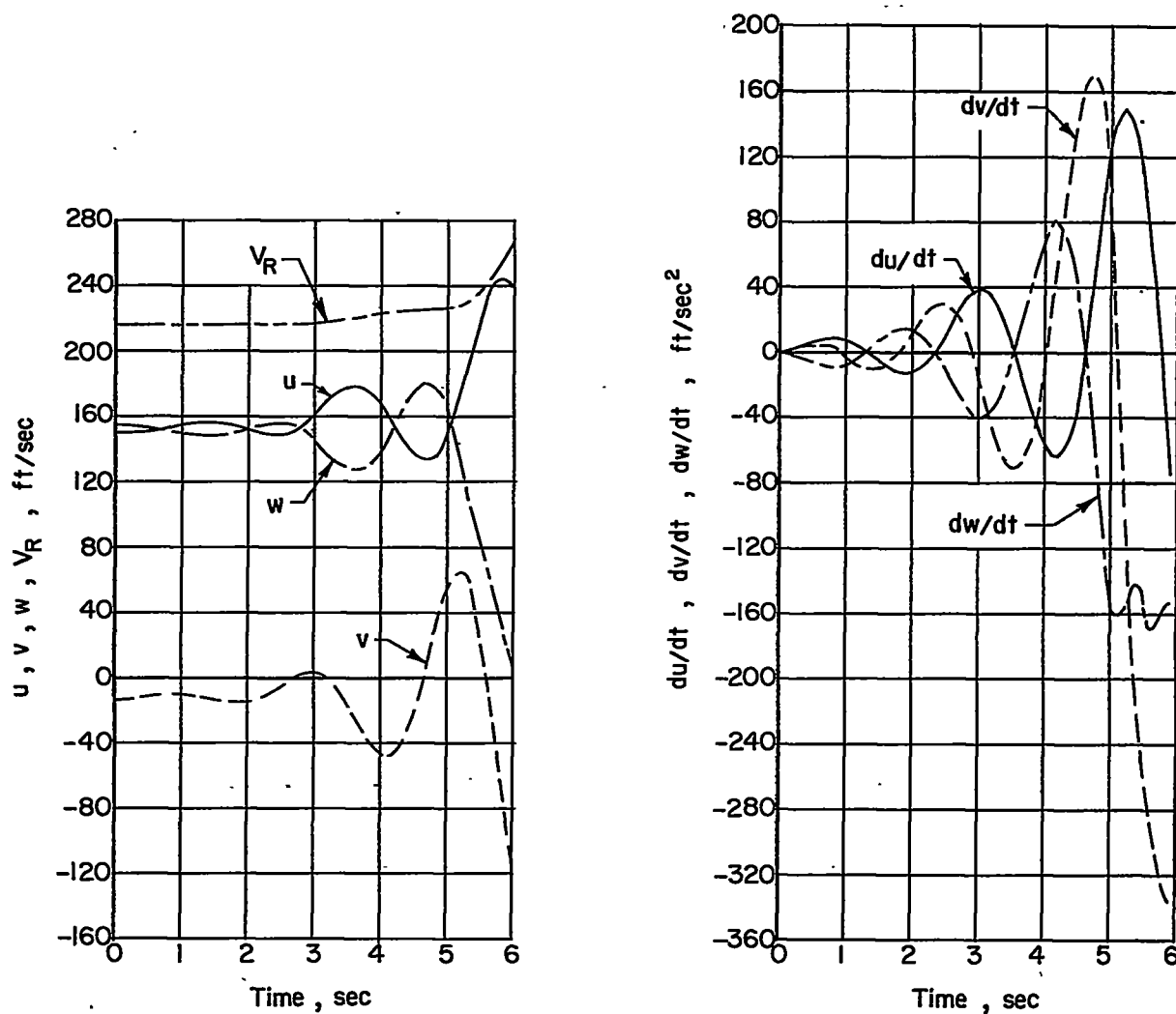


Figure 11.- Calculated variations of linear velocities and accelerations with time during recovery motion.

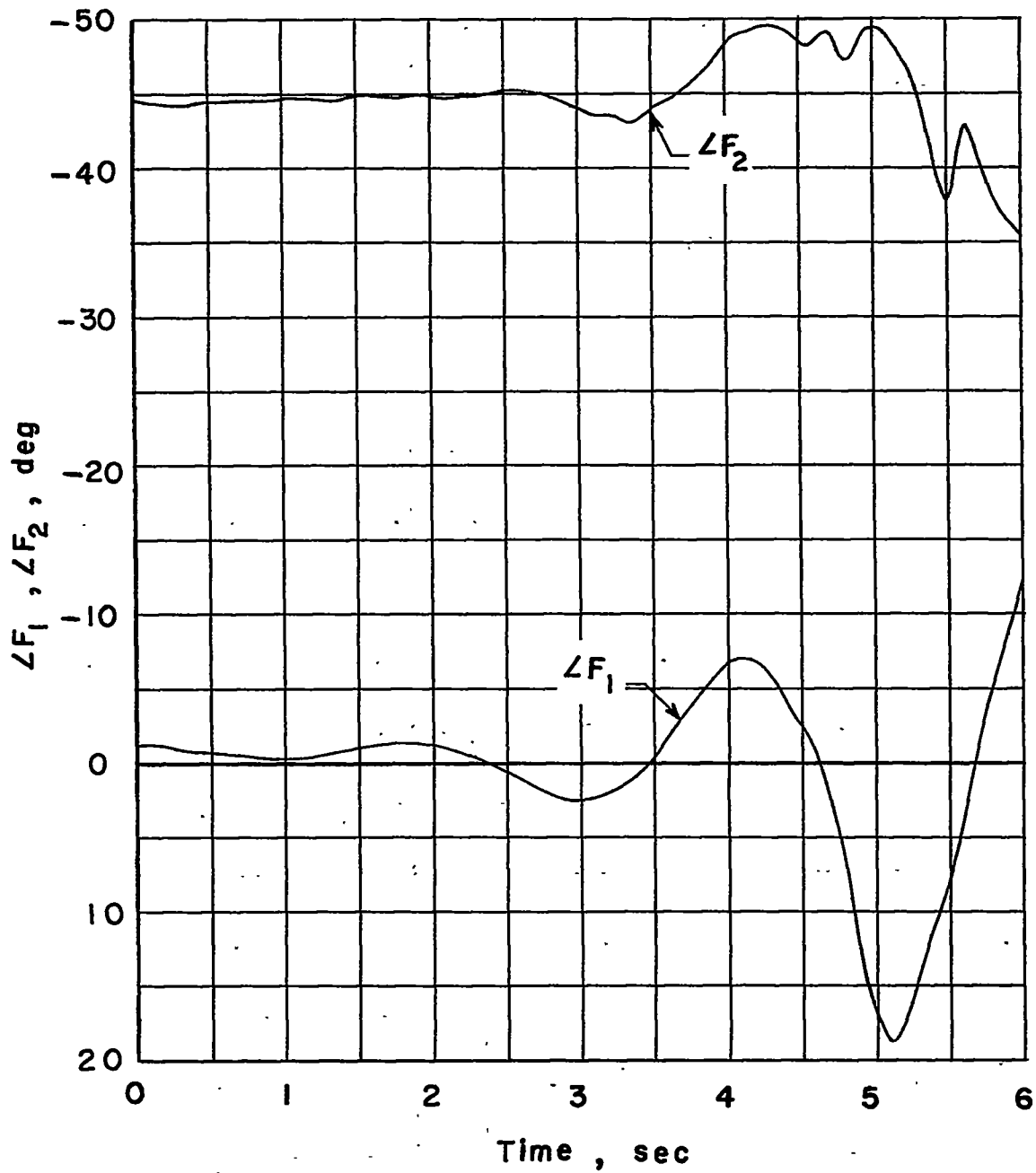


Figure 12.- Calculated variations of  $\Delta F_1$  and  $\Delta F_2$  with time during recovery motion.

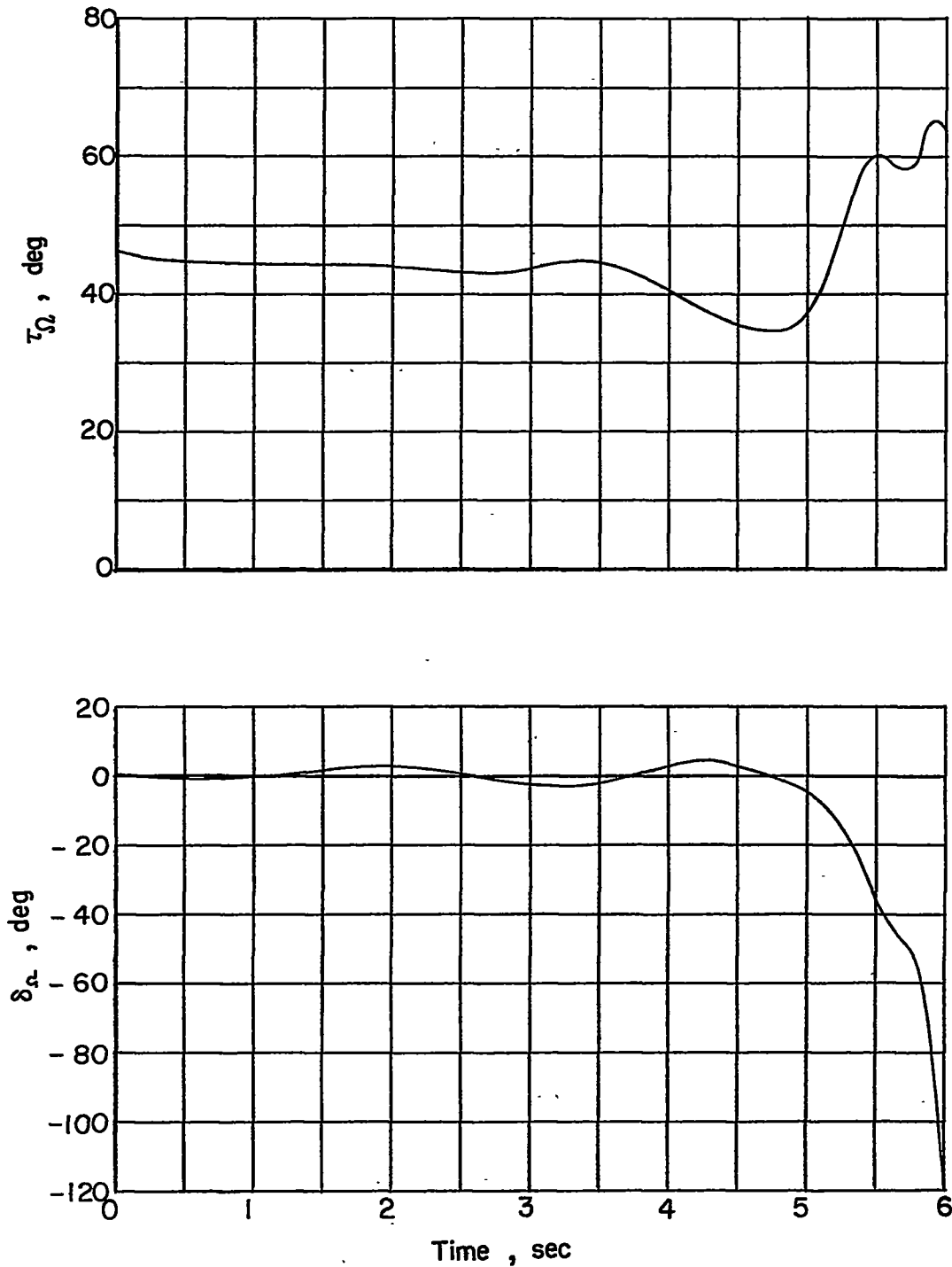


Figure 13.- Calculated variations of  $\tau_{\Omega}$  and  $\delta_{\Omega}$  with time during recovery motion.  $\tau_{\Omega} = \sin^{-1} \frac{r}{\Omega}$ ;  $\delta_{\Omega} = \sin^{-1} \frac{q}{\sqrt{p^2 + q^2}}$ .

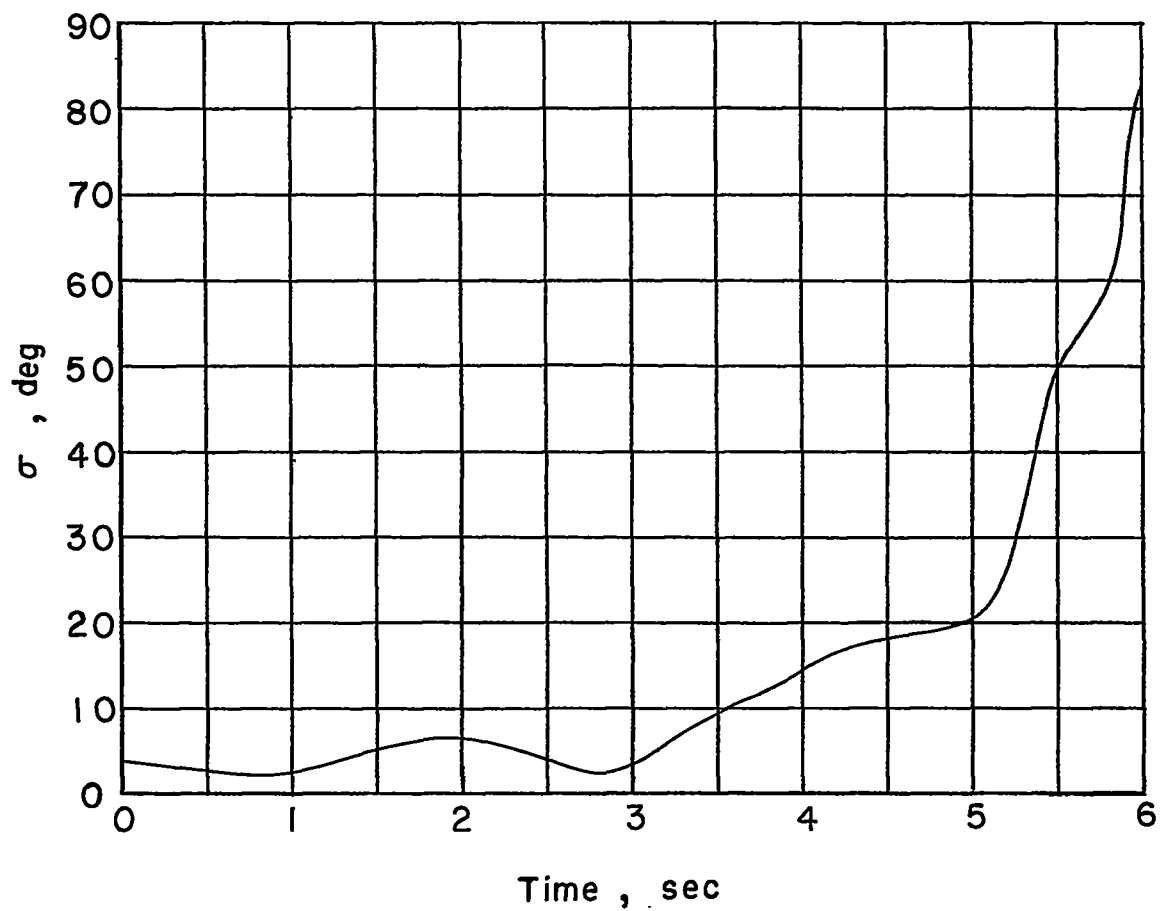


Figure 14.- Calculated variation of  $\sigma$  with time during recovery motion.

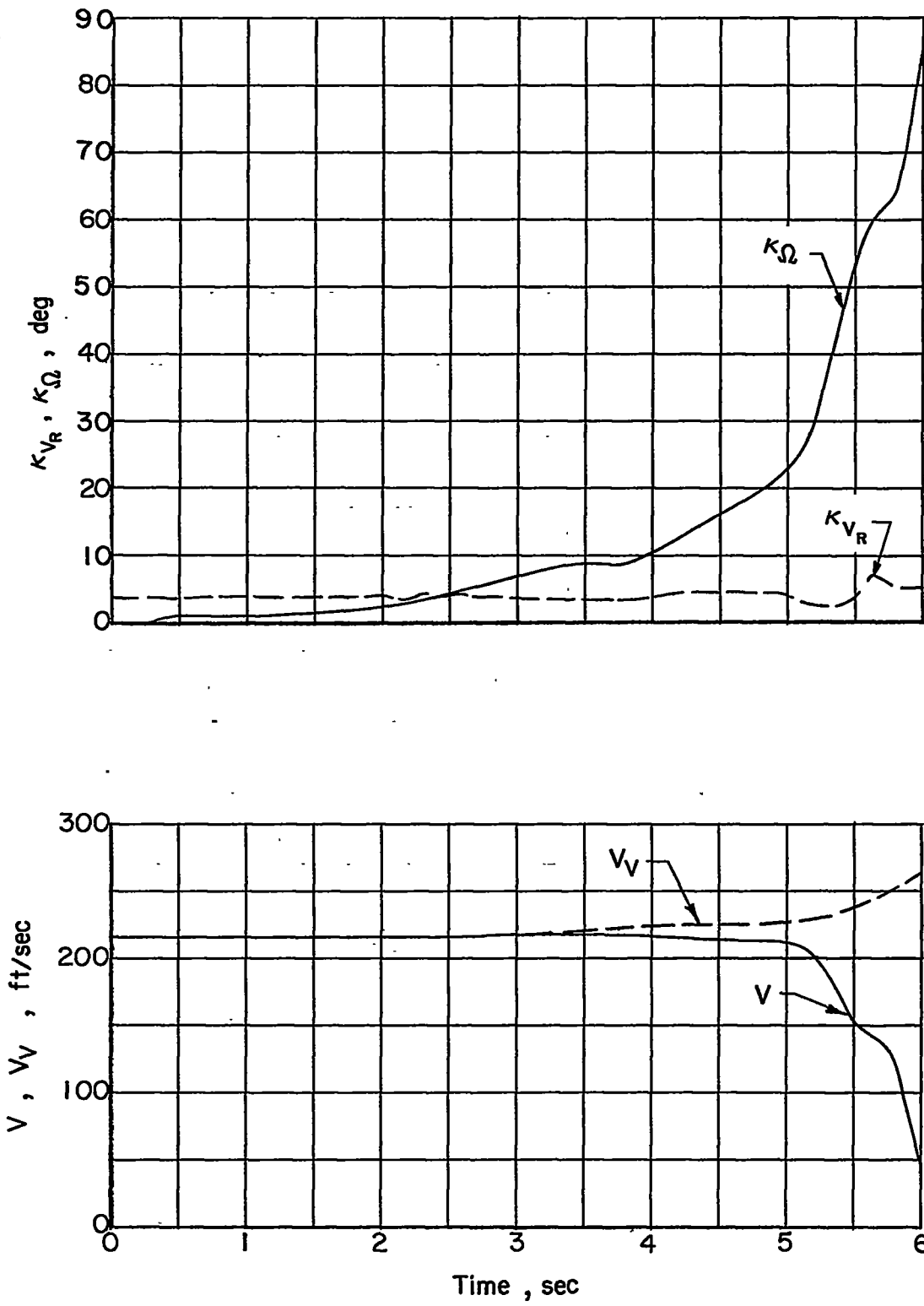


Figure 15.- Calculated variations of  $V_V$ ,  $V$ ,  $\kappa_{V_R}$ , and  $\kappa_{\Omega}$  with time during recovery motion.